THE JOURNAL OF PHYSICAL CHEMISTRY C
A JOURNAL OF THE AMERICAN CHEMICAL SOCIETY

pubs.acs.org/JPCC
Article

Stability of Tin-Containing Hybrid Perovskites: The Thermal Decomposition of Formamidinium Tin Triiodide ($FASnI_3$) Investigated by Thermogravimetry and Effusion Techniques

Martina Pesci, Lorenza Romagnoli,* Bruno Brunetti, Stefano Vecchio Ciprioti, Andrea Ciccioli,* and Alessandro Latini*

Cite This: J. Phys. Chem. C 2025, 129, 9291−9301

Read Online

ACCESS | Metrics & More | Article Recommendations | Supporting Information

ABSTRACT: The gas-releasing thermal decomposition processes of formamidinium tin triiodide perovskite ($CN_2H_5SnI_3$, usually denoted as $FASnI_3$ or, briefly, FASI) were investigated in order to obtain information on the temperature at which decomposition begins and on the nature of the gas species emitted under heating. Results of thermogravimetry-differential thermal analysis (TG-DTA), thermogravimetry-differential scanning calorimetry (TG-DSC), and Knudsen effusion mass spectrometry (KEMS) experiments are presented. TG measurements showed that mass loss starts at temperatures much lower than those of the lead-based corresponding compound $FAPbI_3$, with incipient loss at temperatures as low as 423 K. Unlike $FAPbI_3$, practically no residue is left at T = 823 K. KEMS experiments showed a measurable release of $SnI_4(g)$ occurring from temperatures as low as 318 K, with a $SnI_4(g)$ pressure much lower than the vapor pressure of pure SnI_4, suggesting the presence in the solid of Sn(IV) at reduced activity. At higher temperatures (T > 390 K), the release of $SnI_2(g)$ and various species coming from the organic portion, such as formamidine, hydrogen iodide, ammonia, triazine, and hydrogen cyanide, is observed. For the first time, thermal decomposition of FASI was shown to occur with release of both organic and inorganic (tin iodides) species, with the partial oxidation of Sn(II) to Sn(IV) significantly decreasing the decomposition onset temperature. Finally, based on TG measurements at various scan rates, a kinetic analysis of FASI decomposition was performed, using integral and incremental isoconversional methods, to derive parameters useful for lifetime prediction. Reasonable reaction time values to achieve a low degree of conversion (less than 0.25) were extrapolated at temperatures typically involved in the operation of photovoltaic devices (333 to 353 K).

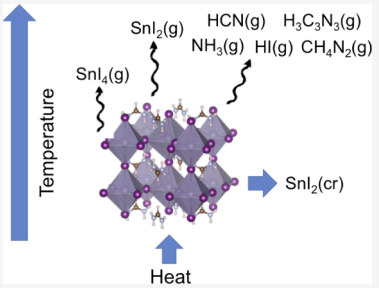

1. INTRODUCTION

While the need to reduce CO_2 emissions, in order to realize the goal of net zero emissions by 2050, is increasingly urgent, solar photovoltaic electricity generation is expected to surpass hydropower and become the largest renewable power source in 2029, according to the International Energy Agency forecasts.[1] This implies, among other things, reducing costs for photovoltaic cell materials and manufacturing, to make solar energy exploitation affordable worldwide. Although silicon-based solar panels have become increasingly cheaper in the last decades, thanks especially to the introduction of polycrystalline and amorphous Si, nevertheless the need for extremely high purity and doping still prompts research for new, inexpensive, and easily manufactured semiconductors.

Among the multitude of currently investigated new generation solar cells (so-called third-generation cells, where the first generation is represented by wafer-based and the second by thin-film ones[2]), perovskite solar cells (PSC) have captivated an unprecedented attention, since the first reported example, in 2009, of a solar cell containing hybrid perovskites, $CH_3NH_3PbX_3$ (where X = Br, I).[3] This is due to the extraordinary properties of these semiconductors, which possess not only band gap values in the suitable range for photovoltaics, but also low exciton binding energies, high absorption coefficients, and long charge carrier diffusion lengths.[4] Moreover, perovskites offer very attractive prospects also in terms of material synthesis, since they can be conveniently obtained, as bulk crystals, nanocrystals, and thin films, by various low-temperature solution techniques,[5] in contrast to many other semiconductors.

The other side of the coin is unfortunately represented by commercialization setbacks caused by poor long-term stability of hybrid perovskites, due to heating and to the effect of environmental agents such as water, oxygen, and UV radiation,[6,7] and by health and environmental concerns related to the presence of lead.[8] Nevertheless, various alternatives to

Received: March 19, 2025
Revised: April 28, 2025
Accepted: April 30, 2025
Published: May 10, 2025

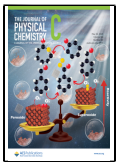

lead have recently gained increasing consideration:[9] for example, Ge- and Sn-based halide perovskites, of general formula ABX_3, Sb- and Bi-based halide perovskites, of general formula $A_3B_2X_9$, and chalcogenide (especially sulfur-containing) perovskites, having general formula $ABCh_3$ (Ch = S, Se). Among all these, however, only tin halide perovskites have hitherto shown comparable (although still inferior) performances and viability to their lead counterparts for solar cells: indeed, the highest certified power conversion efficiency (PCE) on a laboratory scale for a Pb-containing PSC is 26.7%,[10] while the best reported value for Sn-based ones is 15.7%;[11] by contrast, the highest achieved efficiency with bismuth-based perovskites is currently only 3.59%.[12]

The assessment of halide perovskites as really promising candidates for large-scale distribution needs to take into account the possible sources of their detriment under operating conditions. In this regard, great efforts have been conducted in recent years to understand the different facets of lead perovskite instability, for example the effect of heat and light irradiation[13,14] and the thermodynamic[15−17] and kinetic aspects[18,19] of their thermal decomposition.

However, as concerns tin-based perovskites, oxidation of Sn^{2+} to Sn^{4+} is known to constitute a serious issue, causing the formation of undesired vacancies, leading in turn to a self-doping of the material, which makes control of electric properties difficult.[20,21] Although numerous strategies and additives have been devised to mitigate this trouble,[22,23] the problems seem to be inherently unavoidable.[24] Moreover, in contrast to the already mentioned profusion of studies regarding decomposition of lead halide perovskites and despite some recent progress in the comprehension of tin halide perovskite stability,[25−27] information about the degradation mechanisms of the latter is still comparatively limited.

Our work lies in this context and is specifically devoted to investigating the role of Sn(II) → Sn(IV) oxidation in decreasing the thermal stability of formamidinium tin triiodide ($CN_2H_5SnI_3$, FASI in the following), one of the most widely investigated Sn-based perovskites for application in solar cells[28] thanks to the lower volatility of the organic cation, compared to methylammonium. More generally, this study was aimed at elucidating the thermal decomposition pathways of FASI, which were found to be much different from those of the Pb-containing analogue ($CN_2H_5PbI_3$, FAPI in the following). A multitechnique approach, combining effusion techniques, in particular Knudsen effusion mass spectrometry (KEMS), with thermal analysis measurements, was used in this work, similar to that applied by our group to the corresponding Pb-containing material.[29] KEMS measurements allowed the assessment of the gaseous products released from the perovskite upon heating at moderate temperatures, under close-to-equilibrium conditions, and the estimation of partial pressures of the decomposition products. To this end, ancillary experiments were also carried out on binary iodides, SnI_2 and SnI_4. Thermogravimetric analysis of the perovskite and tin iodides, on the other hand, allowed us to determine the onset and the various steps of thermal degradation. Furthermore, by performing TG-DTA at different heating rates and applying the isoconversional method, an overall value for the activation energy of the decomposition reactions was derived.

2. METHODS

2.1. Synthesis. All of the reagents were used as received. Tin powder (99.8%) and formamidinium iodide (≥98%) were supplied by Sigma-Aldrich, iodine (99.9%) was purchased from BDH Chemicals, and CH_2Cl_2 (for analysis, ≥99.9%) and HCl (analytical grade, 37%) were supplied by Carlo Erba Reagents.

2.1.1. Synthesis of SnI_2. SnI_2 was prepared according to a modified literature procedure,[30] by reacting in a round-bottomed flask 5 g of Sn powder with 7 g of I_2 in 30 mL of a 2 M HCl solution, under an argon atmosphere. The suspension was heated to reflux for 2 h until a yellow solution was obtained; then, it was filtered to remove excess Sn and transferred into a conical flask, warmed by a hot water bath. The solution was allowed to cool overnight to room temperature, to facilitate crystallization of the product, and then SnI_2 red crystals were filtered under suction, washed with a degassed 0.02 M HCl solution, and dried at 323 K.

2.1.2. Synthesis of $FASnI_3$. Formamidinium tin triiodide ($CN_2H_5SnI_3$) was synthesized, following a literature procedure,[31] by a solid-state reaction between commercially available formamidinium iodide (CN_2H_5I) and SnI_2: equimolar amounts of the reagents (400 mg of SnI_2 and 194 mg of CN_2H_5I) were ground in an agate mortar for 5 min, until a black powder was formed; the product was inserted in a glass ampule, subsequently evacuated with a rotary vane pump to $\sim 10^{-1}$ mbar, flame sealed, and then transferred in an oven where it was heated for 2 h at 473 K.

2.1.3. Synthesis of SnI_4. For the synthesis of SnI_4, 6 g of Sn powder and 20 g of I_2 were placed in a round-bottomed flask with 40 mL of CH_2Cl_2, and the mixture was heated to reflux for 1 h until the color turned from purple to yellow-orange (indicating the disappearance of I_2), and then quickly filtered while still warm, to remove unreacted tin. The filtered solution was cooled through an ice bath to allow crystallization of the product, and SnI_4 dark-orange crystals were filtered under suction, washed with cold CH_2Cl_2, and dried in the air.

The identity and purity of the compounds were assessed by powder XRD. All of the compounds were obtained in pure crystalline form and used as synthesized, without further purification.

2.2. Powder X-ray Diffraction. Powder X-ray diffraction patterns, in the 20−90° 2θ angular range, of the as-synthesized samples and of $CN_2H_5SnI_3$ residue after KEMS experiments were acquired with a Malvern Panalytical X'Pert Pro MPD diffractometer (Cu Kα radiation, λ = 1.54184 Å), operating in Bragg−Brentano geometry and equipped with an ultrafast X'Celerator RTMS detector. The experiments undertaken in the attempt to study the kinetics of nucleation of SnI_2 (see Section 3.2) were conducted according to the procedure described in ref 29.

2.3. Thermogravimetry-Differential Scanning Calorimetry. Thermogravimetry-differential scanning calorimetry experiments on $CN_2H_5SnI_3$, SnI_2, and SnI_4 were performed with a NEXTA STA200RV Hitachi simultaneous thermal analyzer in alumina crucibles, in the temperature range 298−1073 K, with a heating rate of 10 K·min^{-1}. The analyses were carried out on 10 to 20 mg powder samples under an inert atmosphere (150 mL·min^{-1} @ STP Ar for $CN_2H_5SnI_3$, 100 mL·min^{-1} @ STP N_2 for SnI_2 and SnI_4), and the samples were conditioned for 30 min in the same conditions prior to heating, to avoid oxidation.

2.4. Thermogravimetry-Differential Thermal Analysis. Thermogravimetry-differential thermal analysis measurements of $CN_2H_5SnI_3$ for kinetic analysis through the isoconversional method were performed with a Netzsch STA 409 PC Luxx simultaneous thermal analyzer, in alumina crucibles, in the

https://doi.org/10.1021/acs.jpcc.5c01854
J. Phys. Chem. C 2025, 129, 9291−9301

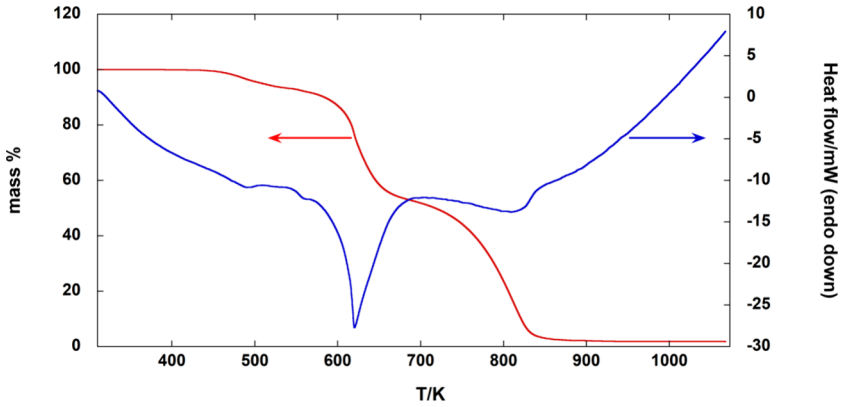

Figure 1. TG-DSC curve of $CN_2H_5SnI_3$ carried out under an Ar atmosphere (150 mL·min^{-1}) at 10 K·min^{-1}.

temperature range 298−773 K, under flowing Ar atmosphere (50 mL·min^{-1} @ STP), using sample mass of about 40 mg, precisely measured. After the sample was weighed, the measurement chamber was quickly evacuated with a rotary vane pump down to a pressure of around 10^{-2} mbar and then refilled with Ar (purity ≥ 99.9995%) up to atmospheric pressure. This procedure was performed to avoid the oxidation of the sample. The heating rates used were 2, 3, 4, 7, and 10 K·min^{-1}.

2.5. KEMS and Knudsen Effusion Mass Loss (KEML). In these techniques, the sample is placed, under high vacuum, in a cylindrical cell equipped with a lid in which a small hole is drilled, allowing the vapor phase to escape under the molecular flow regime.

In KEMS, the vapor effusing from the cell enters the ion source of a mass spectrometer, where neutral species are positively ionized by electron impact, accelerated, separated according to their mass to charge ratio, and finally revealed. In our apparatus,[15,29] a single focusing magnetic sector mass spectrometer is used and ion currents are measured by a secondary electron multiplier. Ions coming from the effusion cell are distinguished from background species by means of a movable shutter placed between the cell and the ion source. Ion intensities, from which partial pressures are obtained (see eq 1 below), are taken as the difference between the total intensity and that measured when the shutter is shifted.

In the experiments described here, a graphite cell with a 1 mm orifice in the lid (also made of graphite) was used. The effusion cell was enclosed in an outer tantalum crucible and was surrounded by a spiral-shaped tungsten heating element. Finally, the crucible and heating coil are surrounded by several tantalum thermal shields. Temperature measurement was carried out through a Pt10%Rh−Pt (type S) thermocouple, placed in a hole made in the bottom of the external tantalum crucible. Ionization energy curves and appearance energies, i.e., the minimum electron energy necessary to produce a given ion, were measured for all of the detected ions. Appearance energies were determined by using the vanishing current method and corrected based on the ionization energy of water,[32] taken as a reference. The energy of the ionizing electron beam was adjusted according to the maximum ionization efficiency of each ion and was in the range 17−24 eV. Partial pressures of the neutral species i in the vapor were calculated from the intensities of the ions produced there from, by eq 1:

$$P_i = \frac{k_{\text{instr}}}{\sigma_i} \sum_k \frac{I_k^+ T \sqrt{M_k}}{a_k} \tag{1}$$

In this equation, I_k^+ represents the ion current of the ion species k (molecular ion or fragment) formed from i under electron impact, M_k is the molecular mass, a_k is the abundance of the observed isotope of the i species, σ_i corresponds to the total ionization cross section, T is the absolute temperature, and k_{instr} is an instrumental constant, corresponding to $\frac{P_{\text{ref}} a_{\text{ref}} \sigma_{\text{ref}}}{I_{\text{ref}}^+ \sqrt{M_{\text{ref}}} T_{\text{ref}}}$, obtained through calibration experiments with a substance of known vapor pressure. Calibration was carried out by vaporizing, in the lower and higher temperature ranges of our experiments, respectively, 1,3,5-triphenylbenzene (powder, 99.9%) and zinc (pieces, 99.9%), both supplied by Sigma-Aldrich.

KEML measurements were carried out with the apparatus described in ref 33. An effusion cell in pyrophyllite was used with a diameter of the effusion hole of 1 mm. In this method, the measured mass loss is related to total vapor pressure P through eq 2:

$$P = K \frac{\mathrm{d}m}{\mathrm{d}t} \sqrt{\frac{2\pi RT}{\bar{M}}} \tag{2}$$

where K is a constant depending on the geometrical characteristics of the effusion hole, $\frac{\mathrm{d}m}{\mathrm{d}t}$ is the rate of mass loss, T is the absolute temperature, and $\bar{M}$ is the average molar mass of the vapor, calculated by eq 3, where x_i is the mole fraction of the i species and M_i its molecular mass:

$$\bar{M} = \left(\sum_i x_i \sqrt{M_i} \right)^2 \tag{3}$$

In this work, KEML was used only to verify if the total pressures were or were not constant at a given temperature.

3. RESULTS

3.1. TG-DSC of $CN_2H_5SnI_3$, SnI_2, and SnI_4. The thermal behavior of FASI was assessed by TG-DSC (Figure 1), performed under an inert atmosphere from room temperature to 1073 K.

The TG curve shows an initial decomposition step, involving about 6.7% mass loss, taking place between 420 and 550 K, followed by a steeper decrease in mass (around −40%) up to about 700 K, characterized by a large endothermic peak. These

https://doi.org/10.1021/acs.jpcc.5c01854
J. Phys. Chem. C 2025, 129, 9291−9301

sequential mass loss steps reproduce qualitatively the behavior already reported in previous TG data from the literature.[31,34−36] Finally, practically all the remaining material is converted into volatile species at 850 K, leaving about 1.7% residue at 1073 K. This thermogravimetric curve can be compared to that of the corresponding lead perovskite.[29] As shown in Figure 2, there is a striking difference between the

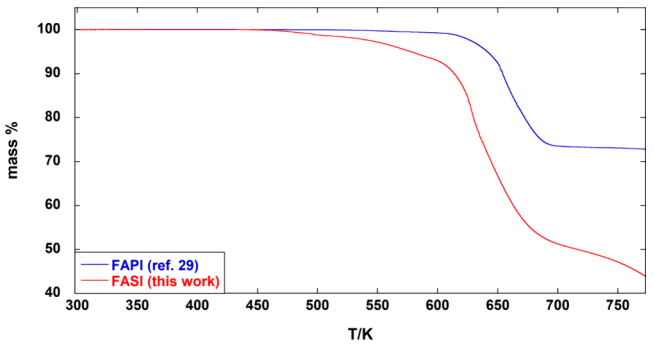

Figure 2. Comparison between TG curves of $CN_2H_5PbI_3$ (FAPI) and $CN_2H_5SnI_3$ (FASI) under an Ar atmosphere at 10 K·min^{-1}.

$CN_2H_5SnI_3$ and $CN_2H_5PbI_3$ thermal behavior, with loss of volatile decomposition products from the latter starting at much higher temperatures, around 570 K. Moreover, the residual mass of 72.8% at 773 K in $CN_2H_5PbI_3$, corresponding to the PbI_2 mass fraction, proves that no Pb-containing gaseous decomposition products are formed below this temperature. By contrast, more than 40% mass of $CN_2H_5SnI_3$ is lost below 700 K, while the CN_2H_5I mass fraction is only 32%, pointing to the formation of volatile Sn-containing degradation products in this temperature range. Although the experimental conditions used in TG and KEMS measurements are very different (higher T range in TG, open pan *vs* Knudsen cell, inert atmosphere *vs* high vacuum), an attempt can be done to explain the observed TG mass loss behavior in light of KEMS findings (see Section 3.3). On this basis, it can be supposed that the thermal behavior below 550 K is due to the release of volatile Sn(IV) species, whereas the mass loss up to about 700 K can be ascribed to the simultaneous evolution of gaseous decomposition products from the organic portion and sublimation of SnI_2 formed as a result of these degradation processes (see eqs 9−11 in Section 4), as mentioned above.

In order to further verify the presence of volatile species from the inorganic component of the perovskite below 700 K, TG-DSC measurements under similar conditions were carried out also on SnI_2 and SnI_4. The resulting curves, shown in Figure 3a and Figure 3b, respectively, are in agreement with previous literature data[37] and draw attention to the much higher volatility of SnI_4 compared to SnI_2. The two endothermic peaks present in both DSC curves are due to the fusion and vaporization of tin iodides. Note that in the TG curve of SnI_2 (Figure 3a), a first mass loss step is observed at a temperature similar to that corresponding to the complete sublimation of SnI_4 (Figure 3b), most probably due to Sn(IV) impurities in the SnI_2 sample. The comparison with the TG curves of $CN_2H_5SnI_3$ provides a confirmation of the previous hypotheses on the decomposition sequence of FASI: the first mass loss step can be attributed, in large part, to the release of Sn(IV) impurities (see Section 4 for more details), while the decomposition step occurring up to about 700 K involves,

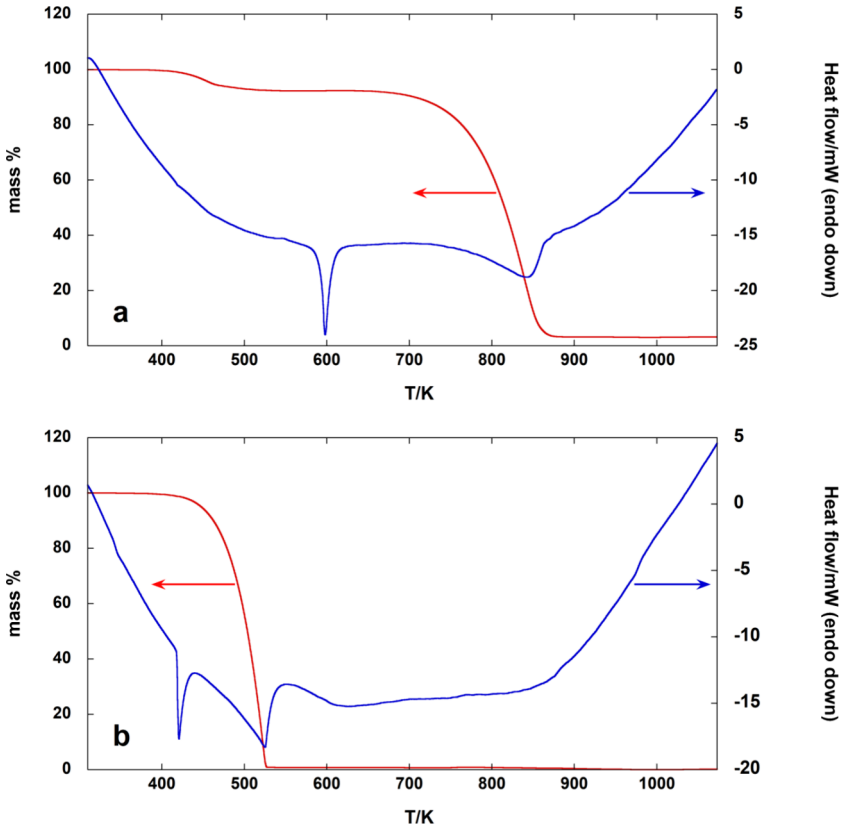

Figure 3. TG-DSC of (a) SnI_2 and (b) SnI_4 carried out under a N_2 atmosphere (100 mL·min^{-1}) at 10 K·min^{-1}.

https://doi.org/10.1021/acs.jpcc.5c01854
J. Phys. Chem. C 2025, 129, 9291−9301

along with decomposition products from the organic portion of $CN_2H_5SnI_3$ as already observed for FAPI,[29] the sublimation of SnI_2 (as results also from KEMS experiments), as evident from the comparison of Figures 1 and 3a (see also Section 3.3). In conclusion, the analysis of the TG curves shows two crucial differences between FASI and FAPI, which can be related (i) to the presence of Sn(IV) impurities in FASI, bringing about the release of the highly volatile Sn(IV) iodide at very low temperature, and (ii) to the higher volatility of solid SnI_2, formed from decomposition of FASI, compared to PbI_2 formed from FAPI.

Finally, a comparison with the TG curve reported in the literature[31] of another tin perovskite, namely, methylammonium tin triiodide (MASI), shows a similar behavior from a qualitative point of view, although with higher mass losses: a first mass loss step (around 20%) probably due to Sn(IV) impurities can be observed for MASI from about 420 K, followed by a much more intense decrease from 620 K, leaving about 15% residual mass at 773 K.

3.2. Kinetic Analysis. Thermal decomposition of materials is often considered as a complex process that involves parallel and consecutive reactions. In TG experiments, the occurrence of a multistep process is usually associated with a shape change of the α vs T curve with varying the heating rate, where α is the degree of conversion, $\alpha\ (T) = (m_i - m_T)/(m_i - m_f)$, with the indices i and f representing the initial and final masses, and m_T the mass at a given temperature T. In the present study, the treatment of TG data to obtain the isoconversional temperatures at different heating rates (see the Supporting Information and Figure S1) is limited to the most significant mass loss between 550 and 700 K (Figure 1) and provides a substantial one-step α vs T curve at each constant heating rate, thus suggesting a simple kinetic description of the process (see below in this section), with no evident multiple-reaction effects. This evidence might seem at variance with the results of KEMS experiments (see Section 3.3 and Section 4.1), which pointed to the occurrence of three parallel decomposition processes (see eqs 9 and 11). However, the kinetic analysis was necessarily performed under conditions very different from those of KEMS. In particular, the degradation mechanism(s) can be significantly affected from effusion *vs* open pan conditions. Furthermore, as evident from Figure S1, the temperature range covered in TG experiments was much higher than that where KEMS spectra were collected. On the other hand, it cannot be excluded that the occurrence of several processes with very similar kinetic properties would result in an apparent one-step shape of α vs T curves.

The basic equation for the kinetic analysis is the general rate equation (GRE):

$$\frac{d\alpha}{dt} = f(\alpha) \times k(T) \tag{4}$$

where $k(T)$ and $f(\alpha)$ are functions depending exclusively on degree of conversion α and temperature, respectively. The temperature function is usually expressed by the Arrhenius equation $k(T) = A\cdot\exp(-E/RT)$. The reaction rate $d\alpha/dt$ is often rearranged to assume the form $d\alpha/dT$, taking into account that TG experiments are almost exclusively performed under a linear heating rate $\beta = dT/dt$: $d\alpha/dT = d\alpha/dt \cdot dt/dT = d\alpha/dt \cdot 1/\beta$.

In the case of a supposed single-step process, a preliminary kinetic approach can be the integral isoconversional method denoted as Kissinger-Akahira-Sunose (KAS),[38] based on the following relationship:

$$\ln(\beta/T^2) = -b(E/RT) + c \tag{5}$$

where b and c are fitting constants independent of temperature. This equation is derived on the assumption of an approximation (Doyle's one[39] is applied in the KAS method) to solve a temperature integral obtained after separation of conversion and temperature variables that has no mathematical solution. As a consequence, activation energy calculated by the slope of the regression lines (one for each defined degree of conversion) must be considered almost constant[40] to consider this method valid.

Alternatively, to have a reliable treatment of data and reasonable results that do not depend on the possible variation of activation energy with the extent of conversion, an incremental isoconversional method (IIM), proposed by Šimon and co-workers,[41] was considered.

The usual plot of the conversion dependence of the activation energy (Figure 4) for the thermal decomposition

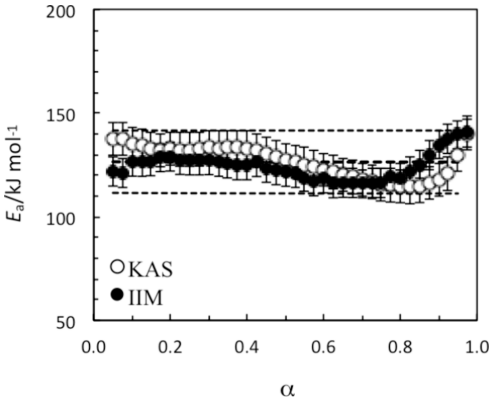

Figure 4. Conversion dependence of the activation energy for the thermal decomposition of FASI according to the two kinetic methods considered.

of FASI revealed the excellent agreement of activation energies derived by KAS and IIM methods within the estimated associated uncertainties. Almost constant E values were obtained between about 110 and 130 kJ·mol^{-1}, which are significantly lower than those obtained for FAPI by using the same method.[29]

On the basis of the above results, the reaction times needed to achieve a given degree of conversion α could be estimated, similarly to what has been recently made for the thermal decomposition of some ionic liquids,[42] using eq 6:

$$t_\alpha = \Sigma_i \Delta t_i = \Sigma_i A_i \times \exp(-E_i/RT) \tag{6}$$

where A_i and E_i are the Arrhenius pair related to the corresponding degree of conversion. In this study, decomposition times of FASI were extrapolated to temperature values (333, 343, and 353 K) much lower compared to the experimental ones, in order to predict the thermal behavior under conditions typically involved in solar cell operation. The reaction time values t_α calculated from the above-described procedure for low degree of conversion ($\alpha < 0.25$) are reported in Figure 5. Despite the rather crude extrapolation involved in the procedure described above, these results can be used for a rough estimate of the degree of the degradation of the light-

https://doi.org/10.1021/acs.jpcc.5c01854
J. Phys. Chem. C 2025, 129, 9291−9301

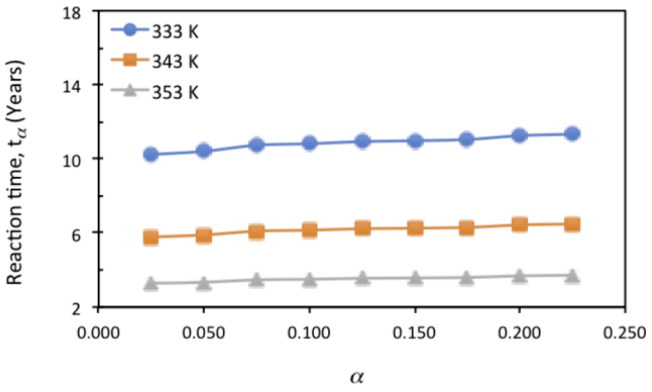

Figure 5. Estimated reaction time t_α for the decomposition process of $CN_2H_5SnI_3$ (FASI) at selected temperatures (333−353 K) for low degrees of conversion.

harvesting material in FASI-containing photovoltaic cells under various temperature conditions.

Besides the isoconversional method based on TG measurements, the kinetic study of the nucleation and growth processes of SnI_2 involved in the decomposition of FASI by temperature-controlled powder X-ray diffraction experiments was also attempted, by using the Johnson−Mehl−Avrami−Kolmogorov (JMAK) model, as performed in the previous work on FAPI.[29] However, different experiments at different but very close temperatures (the useful temperature range in which the kinetics of the decomposition of FASI to SnI_2 and gaseous products could be observed in experimentally reasonable time intervals was 513−531 K, and the temperature difference between each isothermal experiment was 2 K), gave very different values, ranging from 1 to 4, of the Avrami exponent n of the equation:

$$a = 1 - \exp(-kt^n) \quad (7)$$

where a is the volume fraction of the phase SnI_2, k is the kinetic constant, and t is time. Different values of the Avrami exponent n mean different mechanisms of nucleation and growth processes,[43] which is hardly plausible when a sufficiently pure starting material is used in a very narrow temperature range and no phase transitions occur, as verified in the previous work on FAPI. The most plausible explanation lies in the fact that the atmosphere of the nonambient XRD reaction chamber[29] cannot be evacuated, and air can be replaced only by an appropriate gas flow (He in our case); therefore, the process to obtain a reasonably oxygen-free atmosphere after inserting the sample requires many hours. With FASI being extremely prone to oxidation (Sn^{2+} to Sn^{4+}), it is highly probable that the samples, when the XRD experiments were performed, contained significant amounts of Sn^{4+} that influenced in a noncontrollable and nonreproducible way the kinetics of the nucleation and growth processes involved in FASI decomposition. Consequently, the experimental data obtained by temperature-controlled powder X-ray diffraction measurements and their analysis with the JMAK model are not reported in the present work, being of no use, despite the time-consuming experimental and data analysis efforts.

3.3. Partial Pressures of Decomposition Products from Knudsen Effusion Mass Spectrometry. As previously mentioned, we carried out a number of experiments under effusion conditions, i.e., with the sample placed inside a Knudsen cell. The KEMS and KEML techniques (the latter limited to preliminary experiments) were used. In the first method, the effusing vapors are analyzed by a mass spectrometer, whereas in KEML, the mass of the evaporating sample is continuously monitored by a thermobalance, as detailed in Section 2.5.

Preliminary KEML experiments were aimed at verifying if an invariant value of pressure was attained when the FASI sample was heated at a given constant temperature under the effusion conditions. Indeed, a constant value of pressures would suggest the attainment of a thermodynamic heterogeneous equilibrium between the solid and gaseous phases, whereas a continuous change would indicate a corresponding change in activities of the components in the decomposing solid. The results of isothermal KEML experiments shown in Figure S2 point rather to the latter view, with vapor pressures continuously decreasing as the decomposition proceeds. This evidence also discouraged any thermodynamic analysis of partial pressure data derived from the KEMS measurements.

KEMS experiments covered the overall temperature range of 366−462 K. The complete list of the ion species observed in the KEMS spectra is reported in Table 1 with a tentative assignment of neutral precursors.

Table 1. List of Ion Species Detected in KEMS Spectra of $CN_2H_5SnI_3$ with Assigned Neutral Precursors

ion	m/z	neutral species
NH_2^+	16	NH_3
NH_3^+ or OH^+[a]	17	NH_3 or H_2O[a]
H_2O^+[a] or NH_4^+	18	NH_3 or H_2O[a]
CN^+	26	HCN
HCN^+	27	HCN
H_2CN^+	28	$C_3N_3H_3$[b]
$CH_2N_2^+$	42	CH_4N_2[c]
$CH_3N_2^+$	43	CH_4N_2[c]
$CH_4N_2^+$	44	CH_4N_2[c]
$C_2N_2H^+$	53	$C_3N_3H_3$[b]
$C_2N_2H_2^+$	54	$C_3N_3H_3$[b]
$C_3N_3H_3^+$	81	$C_3N_3H_3$[b]
Sn^+	120	SnI_2 and SnI_4
I^+	127	HI, SnI_2, and SnI_4
HI^+	128	HI
SnI^+	247	SnI_2 and SnI_4
SnI_2^+	374	SnI_2 and SnI_4
SnI_3^+	501	SnI_4
SnI_4^+	628	SnI_4

[a]Signal at 18 m/z was found to decrease significantly during the experiment; therefore, H_2O partial pressure was not calculated. [b]Triazine. [c]Formamidine.

In analyzing Table 1, it should be first of all noted that, besides species coming from the decomposition of the organic cation, already observed for FAPI,[29] several Sn−I ions were detected in the vapor produced from FASI, indicating the simultaneous decomposition/release of the inorganic portion in the latter. This result convincingly confirms what was suggested by the TG curves discussed in Section 3.1. To the best of our knowledge, this is the first evidence of this kind of behavior in a tin-based perovskite.

Appearance energies, useful for the identification of neutral precursors of the detected species, were measured for the most intense ions and are reported in Table S1, together with

https://doi.org/10.1021/acs.jpcc.5c01854
J. Phys. Chem. C 2025, 129, 9291−9301

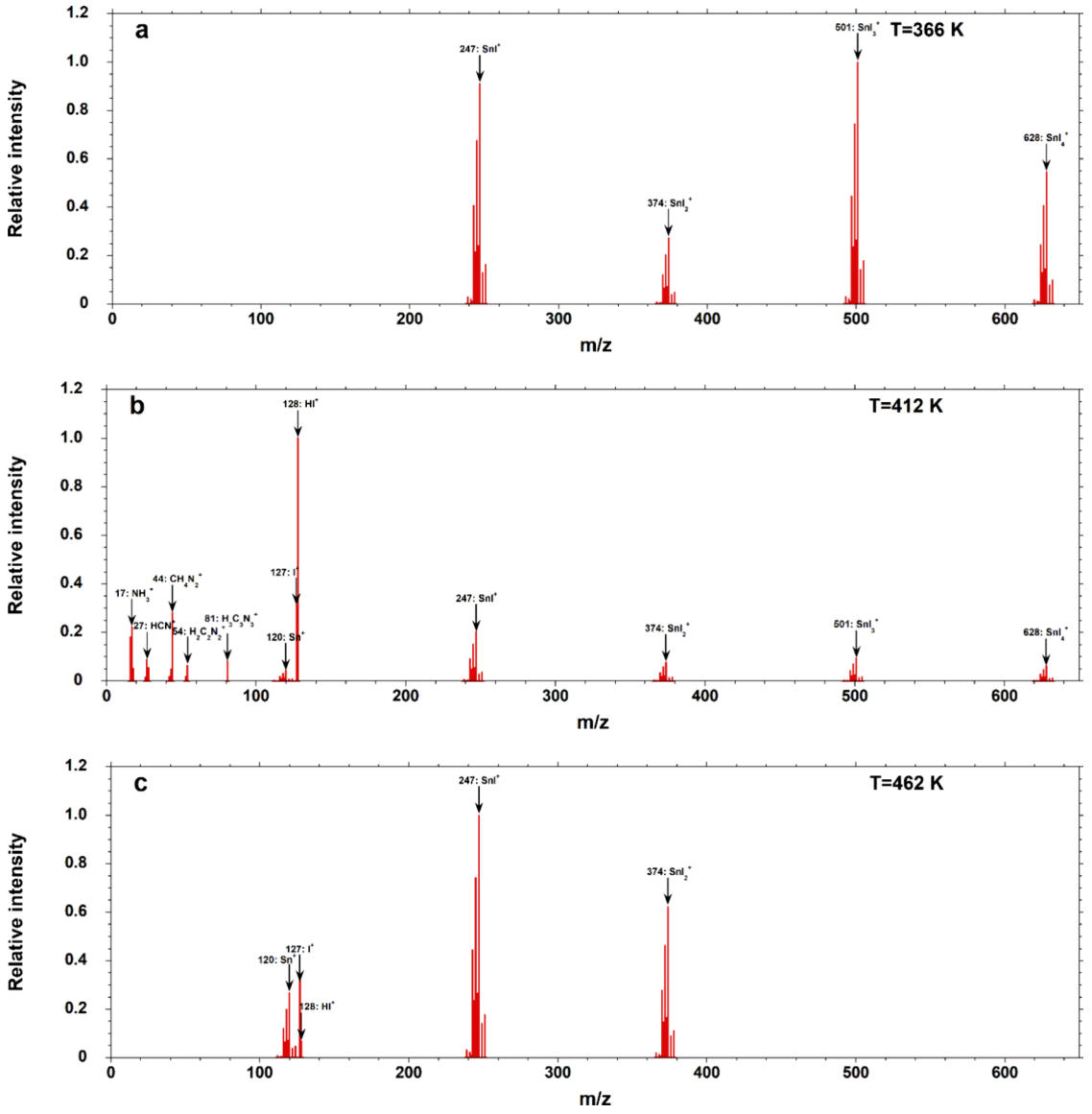

Figure 6. KEMS spectra of the $CN_2H_5SnI_3$ vapors recorded at (a) 366 K, (b) 412 K, and (c) 462 K and increasingly longer vaporization times, from (a) to (c).

ionization energies of the corresponding neutral molecules taken from ref 32, where available.

Several representative mass spectra collected in KEMS experiments are reported in Figure 6a–c. The spectra shown in the figures were recorded at different temperatures and vaporization times. Indeed, it should be noted that the observed signals were found to depend on both variables, consistently with KEML experiments (see again Figure S2). Unlike what one could expect under effusion conditions for a monovariant heterogeneous equilibrium, a stable value of the intensity was not attained at a constant temperature.

In particular, in the first part of any experiment on fresh samples, also corresponding to the lowest temperatures (since the experiments were carried out by gradually increasing the temperature of the effusion cell), only Sn–I ions were detected (namely, SnI^+, SnI_2^+, SnI_3^+, and SnI_4^+), as shown in Figure 6a, where the spectrum at the lowest equilibrated temperature is reported (note that the same ions were already detected at temperatures as low as 318 K). In order to identify the neutral species in the gas phase at this stage, additional vaporization experiments under effusion conditions were performed on SnI_4,[44] at lower temperatures than previously reported studies. The mass spectrum of the vapor phase over pure SnI_4 measured at 324 K is shown as an example in Figure S3. This spectrum revealed the presence of the same Sn–I ions as those originated from $CN_2H_5SnI_3$ thermal decomposition, along with Sn^+, I^+, and I_2^+ (nevertheless, the actual formation of the latter two in the Knudsen cell was questionable, see ref 44). As regards the Sn^+ ion, it is the species with the lowest relative intensity in the SnI_4 KEMS spectrum and probably was not detected in the gas phase of the perovskite at 366 K, due to the overall lower absolute intensity of all the signals in the latter (about two orders of magnitude less than in SnI_4). The mixed Sn–I ion species SnI^+, SnI_2^+, SnI_3^+, and SnI_4^+ exhibited similar relative intensities in the two samples, although SnI_3^+ was the most intense peak in the $CN_2H_5SnI_3$ spectrum at 366 K, while the SnI_4^+ molecular ion was slightly predominant in the SnI_4 spectrum. This analysis led us to reasonably conclude that the only species released by $CN_2H_5SnI_3$ at such low

https://doi.org/10.1021/acs.jpcc.5c01854
J. Phys. Chem. C 2025, 129, 9291–9301

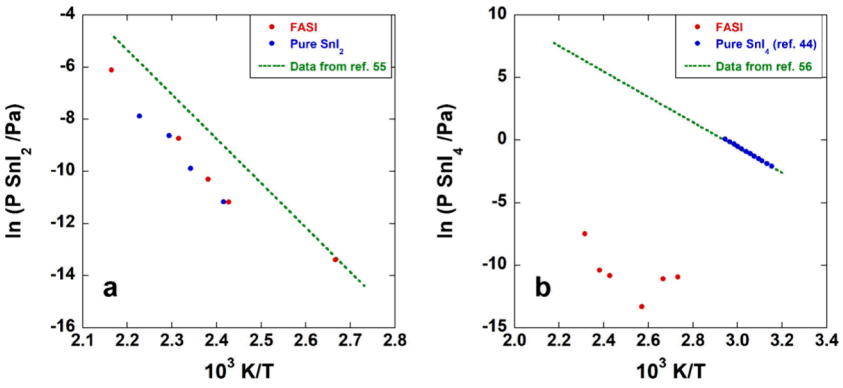

Figure 7. (a) SnI_2 and (b) SnI_4 partial pressures in the $CN_2H_5SnI_3$ gas phase (in red) compared to the vapor pressure of pure compounds (in blue) and literature data (dashed lines).

temperatures and at the initial times of the experiments was gaseous SnI_4.

By increasing the temperature and as the degradation of the sample proceeded, the gas phase was enriched with species arising from the decomposition of the organic component of the perovskite, as can be seen in Figure 6b, where the spectrum recorded at 412 K is reported. This spectrum displays, along with Sn−I ions, already detected at lower temperatures, Sn^+ (with low intensity), I^+, HI^+ (the most intense peak at this temperature), $C_3N_3H_3^+$, $C_2N_2H_2^+$, $CH_4N_2^+$, HCN^+, and NH_3^+, similarly to what had been observed for $CN_2H_5PbI_3$ (although at higher temperatures).[29] From the measured appearance energies (Table S1), $C_2N_2H_2^+$ was attributed to fragmentation of $C_3N_3H_3$, while HCN^+, which could also be a fragment of $C_3N_3H_3$, was considered at least partly as a molecular ion since its appearance energy was found to correspond to the HCN ionization energy. Also, I^+ resulted in a fragment, with an appearance energy almost 3 eV higher than the ionization energy of the I atom (13.2 vs 10.5 eV). This ion could arise from different neutral precursors, namely, HI, SnI_2, and SnI_4 (as explained in the Supporting Information), while NH_3^+, $C_3N_3H_3^+$, and $CH_4N_2^+$ were considered as molecular ions corresponding to ammonia, triazine, and formamidine neutral precursors. The mixed Sn−I ions SnI^+, SnI_2^+, SnI_3^+, and SnI_4^+ showed noticeably different relative intensities compared to those observed in the $CN_2H_5SnI_3$ mass spectrum at 366 K (and also in the SnI_4 KEMS spectrum in Figure S3), with SnI^+ being the most intense peak, pointing to the likely presence of SnI_2 as a neutral species at this temperature. In order to corroborate this hypothesis, KEMS experiments on SnI_2 were also carried out, in the temperature range 414−449 K. The mass spectrum of the vapor phase of SnI_2 at 449 K is reported as an example in Figure S4. In this spectrum (as well as in spectra recorded at different temperatures, which displayed no appreciable temperature dependence of the intensity pattern), SnI^+ is indeed the most intense peak among the Sn−I mixed species. In conclusion, the similarities with the SnI_2 fragmentation pattern and the low relative intensities of SnI_3^+ and SnI_4^+, which must be entirely attributed to the SnI_4 neutral species, provided confirmation of the simultaneous presence of SnI_2 and SnI_4 in the $CN_2H_5SnI_3$ vapor phase in the medium temperature range of our experiments.

Lastly, the spectrum reported in Figure 6c, recorded at the highest temperature of our experiments (462 K), illustrates the composition of the gas phase after prolonged vaporization times, thus when extensive decomposition of the sample had already taken place. Remarkably, it shows the disappearance of SnI_3^+ and SnI_4^+ ions, indicating the disappearance of SnI_4 as a neutral species, as well as that of species produced by the decomposition of the organic portion, except for HI^+, which presents, however, the lowest relative intensity in this spectrum. This led us to the conclusion that the gaseous decomposition products released by $CN_2H_5SnI_3$ at high temperature and after significant thermal degradation are represented essentially by SnI_2, together with very low amounts of residual HI from the organic portion. At this stage, Sn(IV) in the solid was completely depleted, and the organic portion is in large part decomposed and volatilized.

For the calculation of partial pressures of the species produced by $CN_2H_5SnI_3$ thermal decomposition, eq 1 was employed. The procedure used for assignment of intensity contributions to ions that could arise from more than one neutral precursor is discussed in the Supporting Information. From such considerations, it was possible to calculate partial pressures of all the species found in the gas phase produced from $CN_2H_5SnI_3$ thermal decomposition, namely, NH_3, HCN, CH_4N_2 (formamidine), $C_3N_3H_3$ (triazine), HI, SnI_2, and SnI_4, in the explored temperature range. Total ionization cross sections, σ_i, necessary for the application of eq 1,[44−54] required some estimations in the case of species for which experimental or computational values were not available in the literature, and this is likely to introduce uncertainties in the obtained pressure values. Details on the estimation of σ_i values are reported in the Supporting Information. The so-determined pressure values are reported in Table S2.

4. DISCUSSION

4.1. Decomposition Pathways of Formamidinium Tin Triiodide. Partial pressures of SnI_2 and SnI_4 measured in the gas phase produced upon $CN_2H_5SnI_3$ thermal degradation (see Table S2) are compared in Figure 7a,b with those measured by vaporization of binary iodides and with thermochemical data from the literature.

From Figure 7a, it is possible to state that SnI_2 is released by $CN_2H_5SnI_3$ with a very similar vapor pressure (red symbols) to that of pure SnI_2 (blue symbols), pointing to the presence, as a decomposition product, of the corresponding solid compound, which undergoes sublimation. We note that vapor pressure values determined in our KEMS experiments resulted to be lower by a factor about 6−7 than those found in the literature, obtained by previous measurements carried out with the same technique.[55] Different methods used for the estimation of

https://doi.org/10.1021/acs.jpcc.5c01854
J. Phys. Chem. C 2025, 129, 9291−9301

ionization cross-section values can partially explain this discrepancy. Conversely, as concerns SnI_4 (see Figure 7b), partial pressures measured in the gas phase produced by the perovskite are dramatically lower than vapor pressures of pure SnI_4 (around five orders of magnitude), which in this case are in agreement with data from the IVTANTHERMO thermochemical database.[56] This evidence indicates that SnI_4 is not formed as a pure phase in the solid and may be explained with a low thermodynamic activity of Sn(IV) in the decomposing perovskite, bringing about a much lower partial pressure of SnI_4. Since this compound is most probably produced in the gas phase as a consequence of the presence of Sn(IV) ions "dissolved" in the perovskite structure, it can be expected that the loss rate of SnI_4 from the solid is strongly dependent on their concentration, in turn depending on the synthesis and storage conditions. Further evidence for this picture was provided by XRD analysis of the solid residue after KEMS in comparison with the pattern of pristine $CN_2H_5SnI_3$ and SnI_2. As shown in Figure 8, the only crystalline phases in

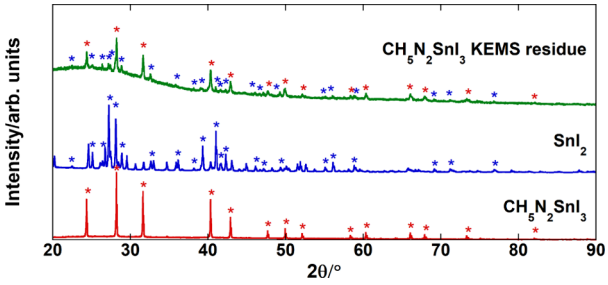

Figure 8. Powder XRD patterns of $CN_2H_5SnI_3$ (in red), SnI_2 (in blue), and the residue after KEMS experiments on $CN_2H_5SnI_3$ up to 432 K (in green).

the residue are the perovskite and SnI_2, with no SnI_4 detected (incidentally, we note that this sample was not subjected to the highest temperatures of our experimental range and that a sample heated for longer times and up to 462 K revealed almost complete amorphization from XRD analysis).

We can thus conclude that a first degradation channel of FASI, observed already at temperatures lower than those reached during solar cell operations, is represented by

$$Sn(IV)(ss) + 4I^- \rightarrow SnI_4(g) \quad (8)$$

where "ss" stands for "solid solution" (tetravalent tin dissolved in the perovskite structure). This offers further confirmation of the key role played by Sn(II) to Sn(IV) oxidation in the degradation of tin-based perovskites, already pointed out in ref 26. To the best of our knowledge, this is the first direct observation of its release as a gaseous decomposition product.

As concerns the species arising from the decomposition of the organic component of $CN_2H_5SnI_3$, the analysis of their partial pressures (see previous section) allowed us to identify different gas-releasing degradation reactions, similar to those previously found to occur in $CN_2H_5PbI_3$[29]:

$$CN_2H_5SnI_3(s) \rightleftharpoons SnI_2(s, g) + CN_2H_4(g) + HI(g) \quad (9)$$

$$CN_2H_5SnI_3(s) \rightleftharpoons SnI_2(s, g) + NH_3(g) + 1/3H_3C_3N_3(g) + HI(g) \quad (10)$$

$$CN_2H_5SnI_3(s) \rightleftharpoons SnI_2(s, g) + NH_3(g) + HCN(g) + HI(g) \quad (11)$$

From the ratios between partial pressures of CH_4N_2 (formamidine) and $H_3C_3N_3$ (triazine) and of CH_4N_2 and HCN, reported in Table S3, it is possible to conclude that both (9) and (10) are favored over (11), which is nonetheless not negligible, and also that (9) is slightly favored over (10) at low temperature. As already highlighted, a striking difference with FAPI, experimentally found for the first time, is represented by the fact that unlike its lead counterpart, for which PbI_2 was found to be produced exclusively as a solid in the temperature range of KEMS experiments, also carried out at higher temperatures, gaseous SnI_2 is released from $CN_2H_5SnI_3$ at temperatures as low as 375 K.

5. CONCLUSIONS

The nature of the gaseous species released from formamidinium tin triiodide (FASI) under heating was, for the first time, investigated in a wide temperature range, in order to identify the different degradation processes of this material under real operating conditions. The thermal decomposition of FASI was found to occur through different pathways with the release of various inorganic and organic species. The first gas species to be released under heating (T > 318 K) was $SnI_4(g)$, providing evidence for the role of tetravalent tin ions/atoms in the degradation of the material under conditions similar to those normally established during photovoltaic operation. The pressure of released $SnI_4(g)$ was measured and compared for the first time to the vapor pressure of pure $SnI_4(s)$, suggesting the presence of low-activity Sn(IV) ions dissolved in the perovskite structure. At higher temperatures (T > 393 K), a number of species were observed in the vapor phase under effusion conditions, indicating the co-occurrence of several decomposition processes:

$$Sn(IV)(ss) + 4I^- \rightarrow SnI_4(g)$$

$$CN_2H_5SnI_3(s) \rightarrow SnI_2(s, g) + CN_2H_4(g) + HI(g)$$

$$CN_2H_5SnI_3(s) \rightarrow SnI_2(s, g) + NH_3(g) + 1/3H_3C_3N_3(g) + HI(g)$$

$$CN_2H_5SnI_3(s) \rightarrow SnI_2(s, g) + NH_3(g) + HCN(g) + HI(g)$$

with the latter process apparently less important compared to the second and third ones. The most abundant species in the vapor phase was found to be HI(g), which is formed in all of the decomposition processes.

The observed behavior is very different from that found in the lead-containing analogue (FAPI), in that the decomposition temperature is significantly lowered for the presence of tetravalent tin, and the vapor phase contains, besides the organic fragments coming from the decomposition of the cationic portion of the compound, also inorganic (tin iodides) species. For the first time, the release of these species in the gas phase from FASI under heating at moderate temperatures was observed. The much higher volatility of Sn(IV) compared to Sn(II) iodide and of SnI_2 compared to PbI_2 makes the thermal degradation pattern of FASI very different from that of FAPI, with important consequences on the feasibility of photovoltaic

https://doi.org/10.1021/acs.jpcc.5c01854
J. Phys. Chem. C 2025, 129, 9291−9301

applications. In order to get a rough estimate of the lifetime of the material under realistic operation temperatures (333 to 353 K), we also performed a kinetic analysis based on thermogravimetry measurements by using the integral and incremental isoconversional methods.

■ ASSOCIATED CONTENT

Supporting Information

The Supporting Information is available free of charge at https://pubs.acs.org/doi/10.1021/acs.jpcc.5c01854.

Details of the kinetic analysis; temperature dependence of the degree of conversion for the decomposition of FASI at different heating rates (Figure S1); mass loss rate measured by KEML at 363 and 393 K (Figure S2); appearance potentials of the ions detected by KEMS (Table S1); KEMS spectra of pure SnI_4 and SnI_2 (Figures S3 and S4); details on the procedures for assignment of neutral precursors of ions in KEMS experiments and for estimation of ionization cross sections; partial pressures of species detected in FASI gas phase (Table S2); and partial pressure ratios between FASI decomposition products (Table S3) (PDF)

■ AUTHOR INFORMATION

Corresponding Authors

Lorenza Romagnoli − *Dipartimento di Chimica, Sapienza University of Rome, Rome 00185, Italy;* orcid.org/0009-0007-6628-1684; Email: lorenza.romagnoli@uniroma1.it

Andrea Ciccioli − *Dipartimento di Chimica, Sapienza University of Rome, Rome 00185, Italy;* orcid.org/0000-0003-1421-8062; Email: andrea.ciccioli@uniroma1.it

Alessandro Latini − *Dipartimento di Chimica, Sapienza University of Rome, Rome 00185, Italy;* orcid.org/0000-0002-3205-4826; Email: alessandro.latini@uniroma1.it

Authors

Martina Pesci − *Dipartimento di Chimica, Sapienza University of Rome, Rome 00185, Italy*

Bruno Brunetti − *Istituto per lo Studio dei Materiali Nanostrutturati, Consiglio Nazionale delle Ricerche, Dipartimento di Chimica, Sapienza University of Rome, Rome 00185, Italy*

Stefano Vecchio Ciprioti − *Dipartimento di Scienze di Base ed Applicate per l'Ingegneria (S.B.A.I.), Sapienza University of Rome, Rome 00161, Italy;* orcid.org/0000-0002-7864-4266

Complete contact information is available at: https://pubs.acs.org/10.1021/acs.jpcc.5c01854

Notes

The authors declare no competing financial interest.

■ ACKNOWLEDGMENTS

The work of A.C., A.L., L.R., and S.V.C. was supported by Sapienza Università di Roma with the project titled "Stabilità termodinamica e cinetica di perovskiti ibride "lead-free" per applicazioni fotovoltaiche" (grant number: RM12117A8484C2E0). The work of L.R. was supported by Sapienza Università di Roma with the project titled "Synthesis and stability of environmentally friendly hybrid and inorganic perovskites for optoelectronic applications" (grant number: AR223188B4C5CC77). The contribution of A.C. and A.L. to this study was carried out within the NEST—Network for Energy Sustainable Transition and received funding from the European Union Next-Generation EU (PIANO NAZIONALE DI RIPRESA E RESILIENZA (PNRR)—MISSIONE 4 COMPONENTE 2, INVESTIMENTO 1.3—D.D. 1561 11/10/2022, B53C22004070006). This manuscript reflects only the authors' views and opinions; neither the European Union nor the European Commission can be considered responsible for them. All Sapienza staff within the NEST project participate to this action under the frame of the grant PE2421852F05911E.

■ REFERENCES

(1) *Renewable Energy Consumption* https://www.iea.org/reports/renewables-2024/global-overview#abstract. (accessed Feb 11, 2025).

(2) Pastuszak, J.; Węgierek, P. Photovoltaic Cell Generations and Current Research Directions for Their Development. *Materials* **2022**, *15* (16), 5542.

(3) Kojima, A.; Teshima, K.; Shirai, Y.; Miyasaka, T. Organometal Halide Perovskites as Visible-Light Sensitizers for Photovoltaic Cells. *J. Am. Chem. Soc.* **2009**, *131* (17), 6050−6051.

(4) Green, M.; Ho-Baillie, A.; Snaith, H. The emergence of perovskite solar cells. *Nat. Photonics* **2014**, *8*, 506−514.

(5) Chouhan, L.; Ghimire, S.; Subrahmanyam, C.; Miyasaka, T.; Biju, V. Synthesis, optoelectronic properties and applications of halide perovskites. *Chem. Soc. Rev.* **2020**, *49*, 2869−2885.

(6) Chowdhury, T. A.; Bin Zafar, M. A.; Sajjad-Ul Islam, M.; Shahinuzzaman, M.; Islam, M. A.; Khandaker, M. U. Stability of perovskite solar cells: issues and prospects. *RSC Adv.* **2023**, *13*, 1787−1810.

(7) Kim, H. J.; Han, G. S.; Jung, H. S. Managing the lifecycle of perovskite solar cells: Addressing stability and environmental concerns from utilization to end-of-life. *eScience* **2024**, *4* (2), No. 100243.

(8) Chen, C.-H.; Cheng, S.-N.; Cheng, L.; Wang, Z.-K.; Liao, L.-S. Toxicity, Leakage, and Recycling of Lead in Perovskite Photovoltaics. *Adv. Energy Mater.* **2023**, *13* (14), 2204144.

(9) Wang, Y.; Liu, J.; Liu, Y.; Li, S.; Xu, X.; Lou, Z. Recent advances in lead-free halide perovskites: from synthesis to applications. *J. Mater. Chem. C* **2024**, *12*, 10267−10329.

(10) Green, M. A.; Dunlop, E. D.; Yoshita, M.; Kopidakis, M.; Bothe, K.; Siefer, G.; Hao, X.; Jiang, J. Y. Solar Cell Efficiency Tables (Version 65). *Prog. Photovolt. Res. Appl.* **2025**, *33* (1), 3−15.

(11) Shi, Y.; Zhu, Z.; Miao, D.; Ding, Y.; Mi, Q. Interfacial Dipoles Boost Open-Circuit Voltage of Tin Halide Perovskite Solar Cells. *ACS Energy Lett.* **2024**, *9* (4), 1895−1897.

(12) Hu, W.; He, X.; Fang, Z.; Lian, W.; Shang, Y.; Li, X.; Zhou, W.; Zhang, M.; Chen, T.; Lu, Y.; et al. Bulk heterojunction gifts bismuth-based lead-free perovskite solar cells with record efficiency. *Nano Energy* **2020**, *68*, No. 104362.

(13) Akbulatov, A. F.; Frolova, L. A.; Dremova, N. N.; Zhidkov, I.; Martynenko, V. M.; Tsarev, S. A.; Luchkin, S. Y.; Kurmaev, E. Z.; Aldoshin, S. M.; Stevenson, K. J.; et al. Light or Heat: What Is Killing Lead Halide Perovskites under Solar Cell Operation Conditions? *J. Phys. Chem. Lett.* **2020**, *11* (1), 333−339.

(14) Ma, L.; Guo, D.; Li, M.; Wang, C.; Zhou, Z.; Zhao, X.; Zhang, F.; Ao, Z.; Nie, Z. Temperature-Dependent Thermal Decomposition Pathway of Organic−Inorganic Halide Perovskite Materials. *Chem. Mater.* **2019**, *31* (20), 8515−8522.

(15) Brunetti, B.; Cavallo, C.; Ciccioli, A.; Gigli, G.; Latini, A. On the Thermal and Thermodynamic (In)Stability of Methylammonium Lead Halide Perovskites. *Sci. Rep.* **2016**, *6*, 31896.

(16) Latini, A.; Gigli, G.; Ciccioli, A. A study on the nature of the thermal decomposition of methylammonium lead iodide perovskite, $CH_3NH_3PbI_3$: an attempt to rationalise contradictory experimental results. *Sustainable Energy Fuels* **2017**, *1*, 1351−1357.

(17) Ciccioli, A.; Latini, A. Thermodynamics and the Intrinsic Stability of Lead Halide Perovskites $CH_3NH_3PbX_3$. *J. Phys. Chem. Lett.* **2018**, *9* (13), 3756−3765.
(18) Burwig, T.; Pistor, P. Reaction kinetics of the thermal decomposition of $MAPbI_3$ thin films. *Phys. Rev. Mater.* **2021**, *5*, No. 065405.
(19) Burwig, T.; Heinze, K.; Pistor, P. Thermal decomposition kinetics of $FAPbI_3$ thin films. *Phys. Rev. Mater.* **2022**, *6*, No. 065404.
(20) Yang, W.-F.; Igbari, F.; Lou, Y.-H.; Wang, Z.-K.; Liao, L.-S. Tin Halide Perovskites: Progress and Challenges. *Adv. Energy Mater.* **2020**, *10* (13), 1902584.
(21) Seo, J.; Song, T.; Rasool, S.; Park, S.; Kim, J. Y. An Overview of Lead, Tin, and Mixed Tin−Lead-Based ABI_3 Perovskite Solar Cells. *Adv. Energy Sustainability Res.* **2023**, *4* (5), 2200160.
(22) Zhang, Z.; Wang, L.; Bi, H.; Baranwal, A. K.; Kapil, G.; Sanehira, Y.; Liu, J.; Liu, D.; Shen, Q.; Hayase, S. Enhancement of Efficiency and Stability for Tin Halide Perovskite Solar Cells by Using Improved Doping Method. *Adv. Optical Mater.* **2024**, *12* (2), 2300962.
(23) Galve-Lahoz, S.; Sánchez-Diaz, J.; Echeverría-Arrondo, C.; Simancas, J.; Rodriguez-Pereira, J.; Turren-Cruz, S.-H.; Martinez-Pastor, J. P.; Mora-Seró, I.; Delgado, J. L. Addressing ambient stability challenges in pure $FASnI_3$ perovskite solar cells through organic additive engineering. *J. Mater. Chem. A* **2024**, *12*, 21933−21943.
(24) Chen, L.; Fu, S.; Li, Y.; Sun, N.; Yan, Y.; Song, Z. On the Durability of Tin-Containing Perovskite Solar Cells. *Adv. Sci.* **2024**, *11*, 2304811.
(25) Akbulatov, A. F.; Tsarev, S. A.; Elshobaki, M.; Luchkin, S. Y.; Zhidkov, I.; Kurmaev, E. Z.; Aldoshin, S. M.; Stevenson, K. J.; Troshin, P. A. Comparative Intrinsic Thermal and Photochemical Stability of Sn(II) Complex Halides as Next-Generation Materials for Lead-Free Perovskite Solar Cells. *J. Phys. Chem. C* **2019**, *123* (44), 26862−26869.
(26) Lanzetta, L.; Webb, T.; Zibouche, N.; Liang, X.; Ding, D.; Min, G.; Westbrook, R. J. E.; Gaggio, B.; Macdonald, T. J.; Islam, M. S.; et al. Degradation mechanism of hybrid tin-based perovskite solar cells and the critical role of tin (IV) iodide. *Nat. Commun.* **2021**, *12*, 2853.
(27) Webb, T.; Haque, S. A. A comparison of molecular iodine evolution on the chemistry of lead and tin perovskites. *Energy Environ. Sci.* **2024**, *17*, 3244−3269.
(28) Li, B.; Jayawardena, K. D. G. I.; Zhang, J.; Bandara, R. M. I.; Liu, X.; Bi, J.; Silva, S. M.; Liu, D.; Underwood, C. C. L.; Xiang, Y.; Ma, Y.; Zhang, W.; Silva, S. R. P. Stability of formamidinium tin triiodide-based inverted perovskite solar cells. *Renew. Sust. Energy Rev.* **2024**, *189* (B), No. 114002.
(29) Luongo, A.; Brunetti, B.; Vecchio Ciprioti, S.; Ciccioli, A.; Latini, A. Thermodynamic and Kinetic Aspects of Formamidinium Lead Iodide Thermal Decomposition. *J. Phys. Chem. C* **2021**, *125* (40), 21851−21861.
(30) Howie, R. A.; Moser, W.; Trevena, I. C. The crystal structure of tin(II) iodide. *Acta Crystallogr.* **1972**, *B28*, 2965−2971.
(31) Stoumpos, C. C.; Malliakas, C. D.; Kanatzidis, G. D. Semiconducting Tin and Lead Iodide Perovskites with Organic Cations: Phase Transitions, High Mobilities, and Near-Infrared Photoluminescent Properties. *Inorg. Chem.* **2013**, *52*, 9019−9038.
(32) Linstrom, P. J.; Mallard, W. G., Eds.; *NIST Chemistry WebBook, NIST Standard Reference Database Number 69*; National Institute of Standards and Technology: Gaithersburg MD, 20899. .
(33) Brunetti, B.; Ciccioli, A.; Gigli, G.; Lapi, A.; Misceo, N.; Tanzi, L.; Vecchio Ciprioti, S. Vaporization of the prototypical ionic liquid $BMImNTf_2$ under equilibrium conditions: a multitechnique study. *Phys. Chem. Chem. Phys.* **2014**, *16*, 15653−1566.
(34) Mitzi, D. B.; Liang, K. Synthesis, Resistivity, and Thermal Properties of the Cubic Perovskite NH_2CH = $NH_2SnI_3$and Related Systems. *J. Solid State Chem.* **1997**, *134* (2), 376−381.
(35) Dang, Y.; Zhou, Y.; Liu, X.; Ju, D.; Xia, S.; Xia, H.; Tao, X. Formation of Hybrid Perovskite Tin Iodide Single Crystals by Top-Seeded Solution Growth. *Angew. Chem., Int. Ed.* **2016**, *55* (10), 3447−3450.
(36) Leijtens, T.; Prasanna, R.; Gold-Parker, A.; Toney, M. F.; McGehee, M. D. Mechanism of Tin Oxidation and Stabilization by Lead Substitution in Tin Halide Perovskites. *ACS Energy Lett.* **2017**, *2* (9), 2159−2165.
(37) Sawada, Y.; Suzuki, M. Thermal change of SnI2 thin films: Part 1. *Thermogravimetry. Thermochimica Acta* **1994**, *232* (1), 29−36.
(38) Akahira, T.; Sunose, T. T. Joint Convention of Four Electrical Institutes. *Res. Report Chiba Inst. Technol. (Sci. Technol.)* **1971**, *16*, 22−31.
(39) Doyle, C. D. Estimating isothermal life from thermogravimetric data. *J. Appl. Polym. Sci.* **1962**, *6* (24), 639−642.
(40) Simon, P.; Dubaj, T.; Cibulková, Z. Frequent flaws encountered in the manuscripts of kinetic papers. *J. Therm. Anal. Calorim.* **2022**, *147*, 10083−10088.
(41) Šimon, P.; Thomas, P. S.; Okuliar, J.; Ray, A. S. An incremental integral isoconversional method. *J. Therm. Anal. Calorim.* **2003**, *72*, 867−874.
(42) Ferdeghini, C.; Guazzelli, L.; Pomelli, C. S.; Ciccioli, A.; Brunetti, B.; Mezzetta, A.; Vecchio Ciprioti, S. Synthesis, thermal behavior and kinetic study of N-morpholinium dicationic ionic liquids by thermogravimetry. *J. Mol. Liq.* **2021**, *332*, No. 115662.
(43) Shirzad, K.; Viney, C. A critical review on applications of the Avrami equation beyond materials science. *J. R. Soc. Interface* **2023**, *20* (203), 20230242.
(44) Romagnoli, L.; Almeida, A. R. R. P.; Silva Ferraz, J. M.; Latini, A.; Freitas, V. L. S.; Ribeiro da Silva, M. D. M. C.; Schiavi, P. G.; Vecchio Ciprioti, S.; Ciccioli, A. Thermodynamic study of tin tetraiodide (SnI_4) sublimation by effusion techniques. *J. Chem. Thermodyn.* **2024**, *199*, No. 107348.
(45) Bull, J. N.; Harland, P. W.; Vallance, C. Absolute Total Electron Impact Ionization Cross-Sections for Many-Atom Organic and Halocarbon Species. *J. Phys. Chem. A* **2012**, *116* (1), 767−777.
(46) Hilpert, K. High temperature mass spectrometry in materials research. *Rapid Commun. Mass. Spectrom.* **1991**, *5* (4), 175−187.
(47) Drowart, J.; Chatillon, C.; Hastie, J.; Bonnell, D. High-temperature mass spectrometry: Instrumental techniques, ionization cross-sections, pressure measurements, and thermodynamic data (IUPAC Technical Report). *Pure Appl. Chem.* **2005**, *77*, 683−737.
(48) Pandey, A. N.; Bigotto, A.; Gulati, R. K. Quantum mechanical studies of bond and molecular polarizabilities of gas-phase metal halides. *Acta Phys. Polym., A* **1991**, *80*, 503−520.
(49) Kalugina, Y. N.; Thakkar, A. J. Electric properties of stannous and stannic halides: How good are the experimental values? *Chem. Phys. Lett.* **2015**, *626*, 69−72.
(50) NIST. *Standard Reference Database 107*; https://www.nist.gov/pml/electron-impact-cross-sections-ionization-and-excitationdatabase, (accessed Feb 11, 2025).
(51) Vinodkumar, M.; Dave, R.; Bhutadia, H.; Antony, B. K. Electron impact total ionization cross sections for halogens and their hydrides. *Int. J. Mass Spectrom.* **2010**, *292* (1−3), 7−13.
(52) Pandya, S. H.; Shelat, F. A.; Joshipura, K. N.; Vaishnav, B. G. Electron ionization of exotic molecular targets CN, C_2N_2, HCN, HNC and BF—Theoretical cross sections. *Int. J. Mass Spectrom.* **2012**, *323*−*324*, 28−33.
(53) Gupta, D.; Choi, H.; Singh, S.; Modak, P.; Antony, B.; Kwon, D.-C.; Song, M.-Y.; Yoon, J.-S. Total ionization cross section of cyclic organic molecules. *J. Chem. Phys.* **2019**, *150*, No. 064313.
(54) Bull, J. N.; Harland, P. W. Absolute electron impact ionization cross-sections and polarisability volumes for C2 to C4 aldehydes, C4 and C6 symmetric ethers and C3 to C6 ketones. *Int. J. Mass Spectrom.* **2008**, *273* (1−2), 53−57.
(55) Hilpert, K.; Bencivenni, L.; Saha, B. Molecular Composition and Thermochemistry of Tin(II), Lead(II), and Scandium(III) Iodide Vapours. *Ber. Bunsenges. Phys. Chem.* **1985**, *89*, 1292−1300.
(56) Iorish, V. S.*IVTANTHERMO database-Version 3.0*; Glushko Thermocenter ofRussian Academy of Sciences, 2005.

https://doi.org/10.1021/acs.jpcc.5c01854
J. Phys. Chem. C 2025, 129, 9291−9301